# Geoacoustic and source tracking using particle filtering: Experimental results

Caglar Yardim,[a] Peter Gerstoft, and William S. Hodgkiss

*Marine Physical Laboratory, Scripps Institution of Oceanography, La Jolla, California 92093-0238*

A particle filtering (PF) approach is presented for performing sequential geoacoustic inversion of a complex ocean acoustic environment using a moving acoustic source. This approach treats both the environmental parameters [e.g., water column sound speed profile (SSP), water depth, sediment and bottom parameters] at the source location and the source parameters (e.g., source depth, range and speed) as unknown random variables that evolve as the source moves. This allows real-time updating of the environment and accurate tracking of the moving source. As a sequential Monte Carlo technique that operates on nonlinear systems with non-Gaussian probability densities, the PF is an ideal algorithm to perform tracking of environmental and source parameters, and their uncertainties via the evolving posterior probability densities. The approach is demonstrated on both simulated data in a shallow water environment with a sloping bottom and experimental data collected during the SWellEx-96 experiment. © *2010 Acoustical Society of America.*
[DOI: 10.1121/1.3438475]

## I. INTRODUCTION

Both passive localization and tracking of a moving source, and geoacoustic inversion and uncertainty analysis are important problems in underwater acoustics. In ocean acoustic applications, there is a natural evolution with time of environmental and source location parameters and the corresponding information in the sequentially arriving acoustic data. This makes sequential processing algorithms attractive. In a previous paper[1] we outlined the theory for sequential Monte Carlo or particle filter methods and demonstrated this by tracking ocean environments from synthetic data. The main purpose of this paper is using these geoacoustic filters to track both the moving source parameters and the environmental parameters including their underlying uncertainties. The approach is demonstrated both in simulation and on real data.

Understanding environmental uncertainty is important for sonar performance prediction and for incorporation into algorithms for the detection and tracking of low-level sources. The uncertain environment can be incorporated into detection and sonar performance prediction algorithms using a Bayesian framework.[2–4] Sonar detection performance prediction with uncertain source position using SWellEx-96 experiment data has been presented in Ref. 5.

Geoacoustic inversion algorithms are used to gather information about this unknown environment.[6–9] Some important geoacoustic parameters that describe the shallow water environment include the ocean sound speed profile (SSP) and sediment layer properties such as the thicknesses, sound speeds, attenuation, and densities. Geoacoustic inversion typically provides both parameter estimates and their uncertainties. It often is performed using matched-field processing (MFP) by finding the best match between measured and simulated acoustic fields using a forward model such as a normal mode or a parabolic equation model. To perform geoacoustic inversion successfully, geometric parameters (such as source location) are often included in the set of parameters to be estimated.

Some of the strategies that have been adopted to increase the robustness of MFP source localization to an unknown environment include the optimum uncertain field processor[10] (OUFP) and focalization.[11] Focalization deals with the source localization problem in an unknown environment by including environmental parameters as unknown inversion parameters along with the source parameters and optimizing the parameters using global search techniques. The OUFP marginalizes over the environmental parameters using a prior to obtain the posterior probability density (PPD) of the source parameters. This method effectively averages the source location over all environments, making the MFP source localization robust to environmental uncertainty. This approach also yields a PPD, hence information about uncertainty in the estimates. A comparison of focalization and marginalization is discussed in Ref. 12.

Tracking involves a moving source and hence the ocean environment and the path between the source and receiver are changing with time. Especially in shallow water environments the environmental parameters in the propagation path can change considerably. Therefore, algorithms that can track the environmental parameters and the source are of interest, e.g., Ref. 13.

Tracking filters such as extended Kalman,[1,14–18] unscented Kalman,[1,19] ensemble Kalman filter,[20] and particle filters[1,21] have been used successfully for ocean acoustics. Previous geoacoustic inversion studies have shown that a geoacoustic particle filter (PF) is versatile and robust in tracking environmental changes in ocean acoustic applications. It also has been shown that a geoacoustic PF with

---
[a]Author to whom correspondence should be addressed. Electronic mail: cyardim@ucsd.edu

enough particles can attain a mean square error close to the posterior Cramér-Rao lower bound (CRLB).[1] CRLB provides a limit on the achievable track performance under the current conditions such as the noise level and errors in the model. No estimator can invert the unknown parameters with a mean square error better than the CRLB. Comparing the PF with the CRLB enables us to see if the filter design needs to be improved in case it is far from attaining the CRLB. It also gives a rough estimate of how many particles one may need to have a good particle filter in a geoacoustic and source tracking problem. Here, a geoacoustic PF is combined with source tracking algorithms to achieve real-time geoacoustic and source tracking in changing ocean environments. This enables us to track both the desired environmental parameters along with source parameters such as speed, range and depth.

Since the PF is an evolving set of particles, with each particle representing a possible solution, the PF can track the evolving uncertainty (PPD) in the parameter estimates. Due to the availability of the PPD at each step, it is possible to pick the best particle at each time step as a maximum *a posteriori* solution (similar to focalization) or it is possible to integrate out the environmental parameters to obtain source tracking by marginalization [similar to OUFP (Ref. 10)].

## II. THEORY

Geoacoustic and source tracking requires two dynamic equations: A state equation that models the evolution of the environment and movement of the source, and an acoustic measurement equation that relates the environment and the source location at step $k$ to the acoustic field. The field is usually, but not necessarily, measured across a receiver array. These are given as

$$\mathbf{x}_k = \mathbf{f}(\mathbf{x}_{k-1}) + \mathbf{B}_{k-1}\mathbf{v}_{k-1}, \quad (1)$$

$$\mathbf{y}_k = \mathbf{h}(\mathbf{x}_k) + \mathbf{w}_k = a_k\mathbf{d}(\mathbf{x}_k) + \mathbf{w}_k, \quad (2)$$

where $\mathbf{f}(\cdot)$ is a known function of the state vector $\mathbf{x}_{k-1}$, and $\mathbf{h}(\cdot)$ is the nonlinear function that relates the environmental and source parameters $\mathbf{x}_k$ to the acoustic measurement vector $\mathbf{y}_k$. Hence, $\mathbf{h}(\cdot)$ includes both the unknown source amplitude term $a_k$ and the known forward model $\mathbf{d}(\mathbf{x}_k)$. $\mathbf{v}_k$, $\mathbf{w}_k$, and $\mathbf{B}_k$ are the process/state noise vector, the measurement noise vector, and the scaling matrix, respectively with

$$E\{\mathbf{v}_k\mathbf{v}_i^T\} = \mathbf{Q}_k\delta_{ki},$$

$$E\{\mathbf{w}_k\mathbf{w}_i^T\} = \mathbf{R}_k\delta_{ki},$$

$$E\{\mathbf{v}_k\mathbf{w}_i^T\} = \mathbf{0}, \quad \forall i,k, \quad (3)$$

where $\delta(\cdot)$ is the Dirac delta function, $\mathbf{Q}_k$ and $\mathbf{R}_k$ are the covariance matrices at $k$ for the corresponding noise terms. The scaling matrix $\mathbf{B}_k$ is not needed for the environmental parameters and is taken as the identity matrix $\mathbf{I}_k$. It is needed only in the source motion model that will relate the depth and acceleration errors to depth, position, and velocity errors in Sec. II A.

## A. The state equation: Ocean and acoustic source modeling

The state equation is formed from two blocks. The first one includes the state equation needed for source tracking. The three source parameters (i.e., the source depth, range, and radial speed) are grouped as $\mathbf{s}_k = [z_s\ r_s\ v_s]_k^T$. Using a constant velocity (CV) track model for the source, the first block in the state equation is given by

$$\mathbf{s}_k = \mathbf{F}_{k-1}^{\mathbf{s}}\mathbf{s}_{k-1} + \mathbf{B}_{k-1}^{\mathbf{s}}\mathbf{v}_{k-1}^{\mathbf{s}}, \quad (4)$$

$$\begin{bmatrix} z_s \\ r_s \\ v_s \end{bmatrix}_k = \begin{bmatrix} 1 & 0 & 0 \\ 0 & 1 & \Delta t \\ 0 & 0 & 1 \end{bmatrix} \begin{bmatrix} z_s \\ r_s \\ v_s \end{bmatrix}_{k-1} + \begin{bmatrix} 1 & 0 \\ 0 & \dfrac{\Delta t^2}{2} \\ 0 & \Delta t \end{bmatrix} \begin{bmatrix} v_{z_s} \\ v_{a_s} \end{bmatrix}_{k-1}, \quad (5)$$

where $\Delta t$ is the time between successive measurements, $v_{z_s}$ and $v_{a_s}$ are random variables representing the variation in source depth and acceleration, respectively.[22] The PF allows for any type of PDFs to be used for these two variables. However, small fluctuations around the mean speed for a source moving with a constant velocity can be characterized adequately by a zero-mean Gaussian PDF. Note that, the underlying PDFs for the geoacoustic and source parameters are not Gaussian even though the noise terms $v_{z_s}$ and $v_{a_s}$ are taken as Gaussian.

The PF framework is versatile and other source models can be used depending on the application. The CV model can be replaced with a fixed source model where only depth and range are state variables and speed is included only indirectly as a noise term (similar to the acceleration term used in the CV model) to mitigate the effects in case the source moves. Similarly for more complicated moving targets, a full moving source model can be used where the depth, range, speed, and acceleration are state variables. Unlike the ship-towed source used here, the source also could move in depth. Then the model simply is replaced by one which includes the vertical speed and/or acceleration in addition to the range parameters. In scenarios where it is possible to extract information about the azimuth of the source (e.g., a horizontal receiver array) it is possible to replace the above models with a 2-D motion model.

The second block is the state equation for the environmental parameters. The environmental parameters (water depth, SSP and sediment parameters) at step $k$ are grouped into $\mathbf{m}_k$, see Ref. 1. This model assumes that the rate of change of the environment is slow for each step. Hence, the second block is given by

$$\mathbf{m}_k = \mathbf{F}_{k-1}^{\mathbf{m}}\mathbf{m}_{k-1} + \mathbf{B}_{k-1}^{\mathbf{m}}\mathbf{v}_{k-1}^{\mathbf{m}}, \quad (6)$$

with $\mathbf{F}^{\mathbf{m}} = \mathbf{B}^{\mathbf{m}} = \mathbf{I}$ where $\mathbf{I}$ is the identity matrix, and $\mathbf{v}^{\mathbf{m}}$ is the state noise matrix for the environmental parameters that takes into account the error in the evolution model, i.e., a rapid change in the environment in a step. Even though many environmental parameters are expected to be evolving slowly most of the time, there can be sudden jumps at the boundaries of geological formations, violating the evolution model selected here. To continue tracking the parameters successfully through the sudden jump, the geoacoustic tracking fil-

ters will have to incorporate a state noise term $\mathbf{v^m}$ with a high covariance $\mathbf{Q}_k$. If the change in the state parameters are significantly different than the values given by the state equation, the filters may diverge even with selection of a high $\mathbf{Q}_k$. Divergence in geoacoustic tracking is studied for extended Kalman, unscented Kalman, and particle filters in detail in Ref. [1].

The initial density for the environment and source location $p(\mathbf{x}_0)$ can be obtained by running a Markov chain Monte Carlo geoacoustic inversion at $t=0$.[6,7] Since the PF can operate on nonlinear densities, any PDF can be used.

The state vector that includes both the source and the environmental parameters is given by merging these two blocks. Defining the state vector as $\mathbf{x}_k^T = [\mathbf{s}_k^T \ \mathbf{m}_k^T]$, the state equation is obtained by inserting Eqs. (4) and (6) into Eq. (1) as follows:

$$\begin{bmatrix} \mathbf{s} \\ \hline \mathbf{m} \end{bmatrix}_k = \begin{bmatrix} \mathbf{F}_{k-1}^{\mathbf{s}} & 0 \\ 0 & \mathbf{I} \end{bmatrix} \begin{bmatrix} \mathbf{s} \\ \hline \mathbf{m} \end{bmatrix}_{k-1} + \begin{bmatrix} \mathbf{B}_{k-1}^{\mathbf{s}} & 0 \\ 0 & \mathbf{I} \end{bmatrix} \begin{bmatrix} \mathbf{v^s} \\ \hline \mathbf{v^m} \end{bmatrix}_{k-1}. \quad (7)$$

## B. The measurement equation: Acoustic propagation model

Measurement equation (2) relates the environmental and source model parameters to acoustic measurements. If the receiver configuration is an array, which can be any arbitrary shape, typically vertical or horizontal, a normal mode code can be used. The acoustic field across a vertical line array (VLA) in the range-dependent environment is calculated here by SNAPRD (Refs. 23 and 24) based on adiabatic normal modes assuming the change is gradual. If there are strong variations that cannot be handled by the adiabatic normal mode model, a parabolic equation model can be used instead. For a given state vector $\mathbf{x}$, the acoustic field is computed here by passing the environmental and source parameters (except source speed) to SNAPRD.

## III. GEOACOUSTIC AND SOURCE TRACKING PARTICLE FILTER

The particle filter is a sequential Monte Carlo method that is used to track desired parameters and their underlying PDFs as they evolve both in space and time.[16,22] PFs work well in tracking geoacoustic parameters[1] due to their ability to handle highly nonlinear systems with non-Gaussian densities. In geoacoustic and source tracking, both additive noise terms $\mathbf{v}_k$ and $\mathbf{w}_k$ can adequately be represented by Gaussian PDFs. However, the posterior PDFs of environmental and source parameters are usually non-Gaussian as shown in Refs. 1 and 7. A sequential importance resampling (SIR) (Ref. 25) type PF is adopted here.

The SIR algorithm uses a set of $n_p$ particles $\{\mathbf{x}_k^i\}_{i=1}^{n_p}$ to represent the PDF at each step $k$. The filter has predict and update sections which the SIR algorithm uses first for predicting the next set of values of the environmental and source parameters given their previous history and then including the latest measurement result to correct/update the predicted value and their PDFs. The initial set of particles $\{\mathbf{x}_0^i\}_{i=1}^{n_p}$ are sampled from the prior $p(\mathbf{x}_0)$. The SIR algorithm uses a transitional prior as its importance sampling[26] density,

i.e., $p(\mathbf{x}_k|\mathbf{x}_{k-1},\mathbf{y}_k)=p(\mathbf{x}_k|\mathbf{x}_{k-1})$. This is a popular choice since it is easy to sample from a transition density that does not depend on acoustic measurement $\mathbf{y}_k$. This selection results in particle weights proportional to the likelihood $W_k \propto p(\mathbf{y}_k|\mathbf{x}_k)$. In geoacoustic tracking the complex source amplitude $a_k$ usually is not known. Therefore, this term is estimated with a maximum likelihood (ML) estimator during the likelihood calculation of each particle in the ensemble.[27] An alternate method where the source spectrum is inverted along with the source location can be found in Ref. 28. The PF likelihood formulation with an unknown source signal closely follows that of the classical geoacoustic inversion likelihood obtained from the Bartlett power objective function.[27]

Following Eq. (2), the additive complex Gaussian noise for each frequency $f_j$ and step $k$, $\mathbf{w}_k(f_j)$ is written as $\mathbf{w}_k(f_j) = \mathbf{y}_k(f_j) - a_k(f_j)\mathbf{d}(\mathbf{x}_k,f_j)$ with a corresponding array coherent, multifrequency likelihood function

$$\mathcal{L}(\mathbf{x}_k) = \prod_{j=1}^{n_f} \frac{1}{(\pi \nu_j)^{n_h}} \exp\left[ -\frac{\|\mathbf{y}_k(f_j) - a_k(f_j)\mathbf{d}(\mathbf{x}_k,f_j)\|^2}{\nu_j} \right], \quad (8)$$

where $n_h$ is and $n_f$ are the number of hydrophones and the frequencies used in tracking, and $\nu_j$ is the noise variance at frequency $f_j$. The unknown source is estimated by a maximum likelihood estimator. An analytic solution is obtained by solving $\partial \mathcal{L}/\partial a_k = 0$ as follows:

$$\hat{a}_k(f_j) = \frac{\mathbf{d}(\mathbf{x}_k,f_j)^H \mathbf{y}_k(f_j)}{\|\mathbf{d}(\mathbf{x}_k,f_j)\|^2}. \quad (9)$$

Inserting the source estimate back into Eq. (8) and defining a cross spectral density function $\mathbf{C}_j = E[\mathbf{y}_k(f_j)\mathbf{y}_k(f_j)^H] = \mathbf{h}(\mathbf{x}_k,f_j)\mathbf{h}(\mathbf{x}_k,f_j)^H + \nu_j\mathbf{I}$, the likelihood is written as[27,29]

$$\mathcal{L}(\mathbf{x}_k) = \prod_{j=1}^{n_f} \frac{1}{(\pi \nu_j)^{n_h}} \exp\left[ -\frac{\phi_j(\mathbf{x}_k)}{\nu_j} \right], \quad (10)$$

$$\phi_j(\mathbf{x}_k) = \operatorname{tr} \mathbf{C}_j - \frac{\mathbf{d}(\mathbf{x}_k,f_j)^H \mathbf{C}_j \mathbf{d}(\mathbf{x}_k,f_j)}{\mathbf{d}(\mathbf{x}_k,f_j)^H \mathbf{d}(\mathbf{x}_k,f_j)}, \quad (11)$$

where tr is the trace operation and $\phi_j$ is the Bartlett objective function. Treating the unknown noise variance $\nu_j$ as a nuisance parameter, we can again use a maximum likelihood estimator similar to the unknown source estimation performed above. Solving $\partial \mathcal{L}/\partial \nu_j = 0$ results in[29]

$$\hat{\nu}_j = \frac{\phi_j(\mathbf{x}_k)}{n_h}, \quad (12)$$

$$\mathcal{L}(\mathbf{x}_k) = \prod_{j=1}^{n_f} \left( \frac{n_h}{e \pi \phi_j(\mathbf{x}_k)} \right)^{n_h}. \quad (13)$$

A single iteration at step $k$ of the SIR is summarized as follows.

(1) *Predict.* For a given set of particles from the previous step $\{\mathbf{x}_{k-1}^i\}_{i=1}^{n_p}$, create a new set $\{\mathbf{x}_{k|k-1}^i\}_{i=1}^{n_p}$ by using Eq. (1). Hence, predict where each particle should be at the current step given its previous location and the transition density $p(\mathbf{x}_k|\mathbf{x}_{k-1})$.
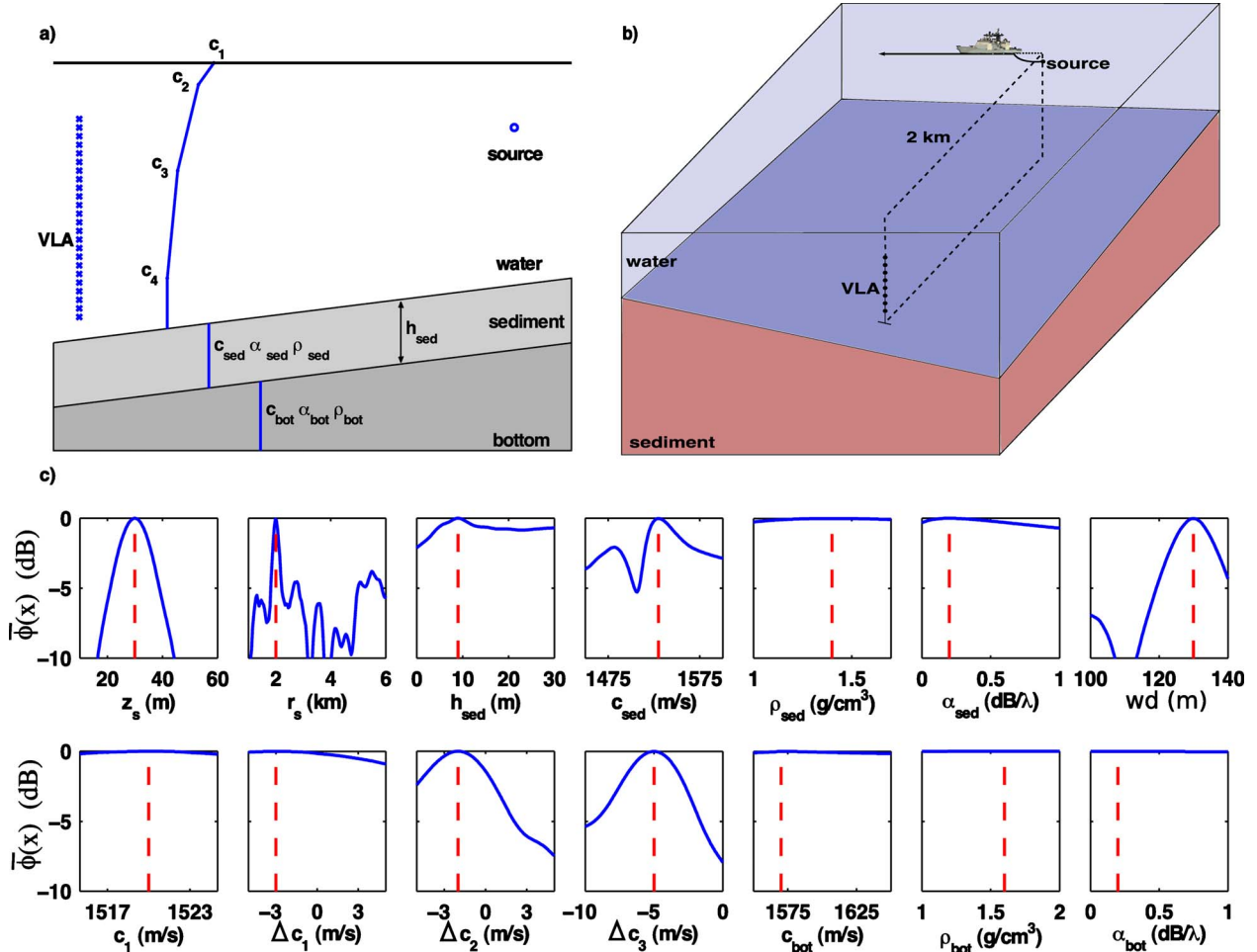
FIG. 1. (Color online) (a) Environmental model used in the simulations, (b) the simulation setup involving a fixed VLA and moving source in a range-dependent environment, and (c) sensitivity plots of geoacoustic parameters at $t=0$.

(2) *Update.* Update the predictions in the previous step using the acoustic data that just came in at the current step $k$. Calculate the normalized weight $W_k^i$ of each particle $\mathbf{x}_{k|k-1}^i$ from its likelihood function

$$p(\mathbf{y}_k|\mathbf{x}_{k|k-1}^i) = \mathcal{L}(\mathbf{x}_{k|k-1}^i) = \prod_{j=1}^{n_f} \left( \frac{n_h}{e\pi\phi_j(\mathbf{x}_{k|k-1}^i)} \right)^{n_h}, \qquad (14)$$

$$W_k^i = \frac{p(\mathbf{y}_k|\mathbf{x}_{k|k-1}^i)}{\sum_{i'=1}^{n_p} p(\mathbf{y}_k|\mathbf{x}_{k|k-1}^{i'})}. \qquad (15)$$

The posterior PDF $p(\mathbf{x}_k|\mathbf{x}_{k-1}, \mathbf{y}_k)$ (and any other desired result) can now be approximated using importance sampling

$$p(\mathbf{x}_k|\mathbf{x}_{k-1}, \mathbf{y}_k) = \sum_{i'=1}^{n_p} W_k^{i'} \delta(\mathbf{x}_k - \mathbf{x}_k^{i'}). \qquad (16)$$

(3) *Resample.* Create a new set of particles denoted by $\{\mathbf{x}_{k|k}^i\}_{i=1}^{n_p}$ by resampling $\{\mathbf{x}_{k|k-1}^i\}_{i=1}^{n_p}$, effectively integrating both the predictions from previous values and the information coming from the new measurement. Resampling generates particles with identical weights from the parent set according to the weights of the parent particles, with high likelihood particles generating more particles than the low likelihood ones.[22]

## IV. EXAMPLES

This section provides two examples. The first is a synthetic geoacoustic and source tracking simulation in a sloping shallow water environment with small variations in other environmental parameters and a moving source. The purpose of the simulation is to demonstrate how the PF tracks the uncertainties in parameters as PPDs. The second tracking example analyzes data collected during the SWellEx-96 experiment in a similar environment as in the simulation.

### A. Simulated data in a sloping bottom

This section presents a synthetic geoacoustic and source tracking example in a sloping bottom, shallow water environment. The model parametrization includes the water depth, SSP, sediment and bottom parameters, see Fig. 1(a). The model, the starting environmental parameters and the VLA are taken similar to Ref. 13. The environmental parameters include sediment thickness $h_{\text{sed}}$, sound speed, density, and attenuation for both sediment and bottom layers, the water depth at the source location $w_d$, and a four-parameter SSP ($c_1-c_4$ at depths of 0, 10, 50, and 100 m). Instead of the actual sound speed values, the difference between layer sound speeds are used to reduce the inter-parameter correlation. The state vector includes $c_1$, $\Delta c_1 = c_1 - c_2$, $\Delta c_2 = c_2 - c_3$,

Yardim *et al.*: Geoacoustic and source tracking

TABLE I. Environmental parameters.

| | $\mathbf{x}$ | $\mathbf{x_0}$ | $\mathbf{P_0}^{1/2}$ | State noise, $\mathbf{Q}_k^{1/2}$ | L. bound | U. bound |
|---|---|---|---|---|---|---|
| Source | $z_s$ (m) | 30 | 0.2 | 0.2 | 1 | 100 |
| | $r_s$ (m) | 2000 | 50 | $0.025 \times \dfrac{\Delta t^2}{2}$ | 500 | 8000 |
| | $v_s$ (m/s) | 0 | 0.01 | $0.025 \times \Delta t$ | 0 | 10 |
| Water | $c_1$ (m/s) | 1520 | 0.15 | 0.15 | 1515 | 1525 |
| | $\Delta c_1$ (m/s) | $-3$ | 0.15 | 0.15 | $-5$ | 5 |
| | $\Delta c_2$ (m/s) | $-2$ | 0.15 | 0.15 | $-5$ | 5 |
| | $\Delta c_3$ (m/s) | $-5$ | 0.15 | 0.15 | 0 | 10 |
| | $w_d$ (m) | 130 | 0.8 | 0.8 | 80 | 150 |
| Sediment | $c_{sed}$ (m/s) | 1530 | 0.25 | 0.25 | 1450 | 1600 |
| | $h_{sed}$ (m) | 9 | 0.25 | 0.25 | 0 | 30 |
| | $\rho_{sed}$ (g/cm$^3$) | 1.4 | 0.005 | 0.005 | 1 | 1.7 |
| | $\alpha_{sed}$ (dB/$\lambda$) | 0.2 | 0.005 | 0.005 | 0 | 1 |
| Bottom | $c_{bot}$ (m/s) | 1570 | $\cdots$ | $\cdots$ | 1550 | 1650 |
| | $\rho_{bot}$ (g/cm$^3$) | 1.6 | $\cdots$ | $\cdots$ | 1 | 2 |
| | $\alpha_{bot}$ (dB/$\lambda$) | 0.2 | $\cdots$ | $\cdots$ | 0 | 1 |

and $\Delta c_3 = c_3 - c_4$. Water depth at the VLA is 130 m. The environmental parameters, their start values and prior standard deviations ($\mathbf{x}_0$ and $\mathbf{P_0}^{1/2}$), state noise $\mathbf{Q}_k$, lower and upper bounds of parameters are given in Table I. Since this is a simulation, the true values of all of these parameters are readily available. However, in real applications some of these may not be known or computed from the data. Then the values that will result in good track performance will need to be found by what is referred to as tuning of the filter. A more detailed discussion can be found in Ref. 16. The purpose of the current selection of ocean parameters is to test the abilities of the PF under substantial environmental change.

The setup and the movement of the source are shown in Fig. 1(b). The simulation starts at a source range of 2 km with the source moving at a constant velocity of 5 m/s perpendicular to the source-VLA plane. Hence, the radial source speed $v_s = 0$ at $t = 0$, slowly increasing and converging toward the full ship velocity of 5 m/s ($\sim$10 kn) as the ship moves. The received acoustic field across the VLA contains information about source depth $z_s$, range $r_s$, and $v_s$. Due to the large initial radial acceleration, which slowly decreases as the ship moves further, the CV track model in Eq. (5) is not accurate. Thus, the acceleration error $v_{a_s}$ in Eq. (5) must compensate for the error in the evolution model.

The simulation parameters are given in Table II. Four frequencies (200, 275, 350, and 425 Hz) are used with 20 s between measurements for 40 time steps ($k = 1, \ldots, 40$) resulting in a total track length of 13.3 min during which the ship travels from 2 to 4.38 km radial range. The element signal to noise ratio (SNR) (Ref. 13)

$$\text{SNR} = 10 \log \frac{[a_k \mathbf{d}(\mathbf{x_k})]^H [a_k \mathbf{d}(\mathbf{x}_k)]}{\mathbf{w}_k^H \mathbf{w}_k} \qquad (17)$$

starts at 8.8 dB at 2 km and decreases with range as shown in Table II.

Water depth is taken as a fully range-dependent, time-evolving parameter. The SSP and sediment parameters are taken as range-independent but they change with time as the ship moves, representing the changing average values of the SSP and sediment parameters between the VLA and the new source position. For the simulation, this time evolution is created using the state noise $\mathbf{Q}_k$ and the state equation. Water depth at source location ($w_d$) starts at 130 m, same as the water depth at the VLA location, and decreases to 100 m as the ship moves. Other environmental parameters and source depth fluctuate in time as first order Markov chains following Eq. (1) with variances given by the diagonal elements of $\mathbf{Q}_k$.

A sensitivity analysis is carried out to assess which environmental parameters affect the acoustic field at $t = 0$, see Fig. 1(c). Each sensitivity curve is created by sweeping one parameter at a time, keeping the others constant at their values at $t = 0$. Even though this simulation does not fully reflect the real multi-dimensional sensitivity, it still provides guidance about which of these parameters are insensitive to acoustic field across the array. The results for the selected environmental model in Fig. 1(b) show that the acoustic field

TABLE II. Simulation parameters.

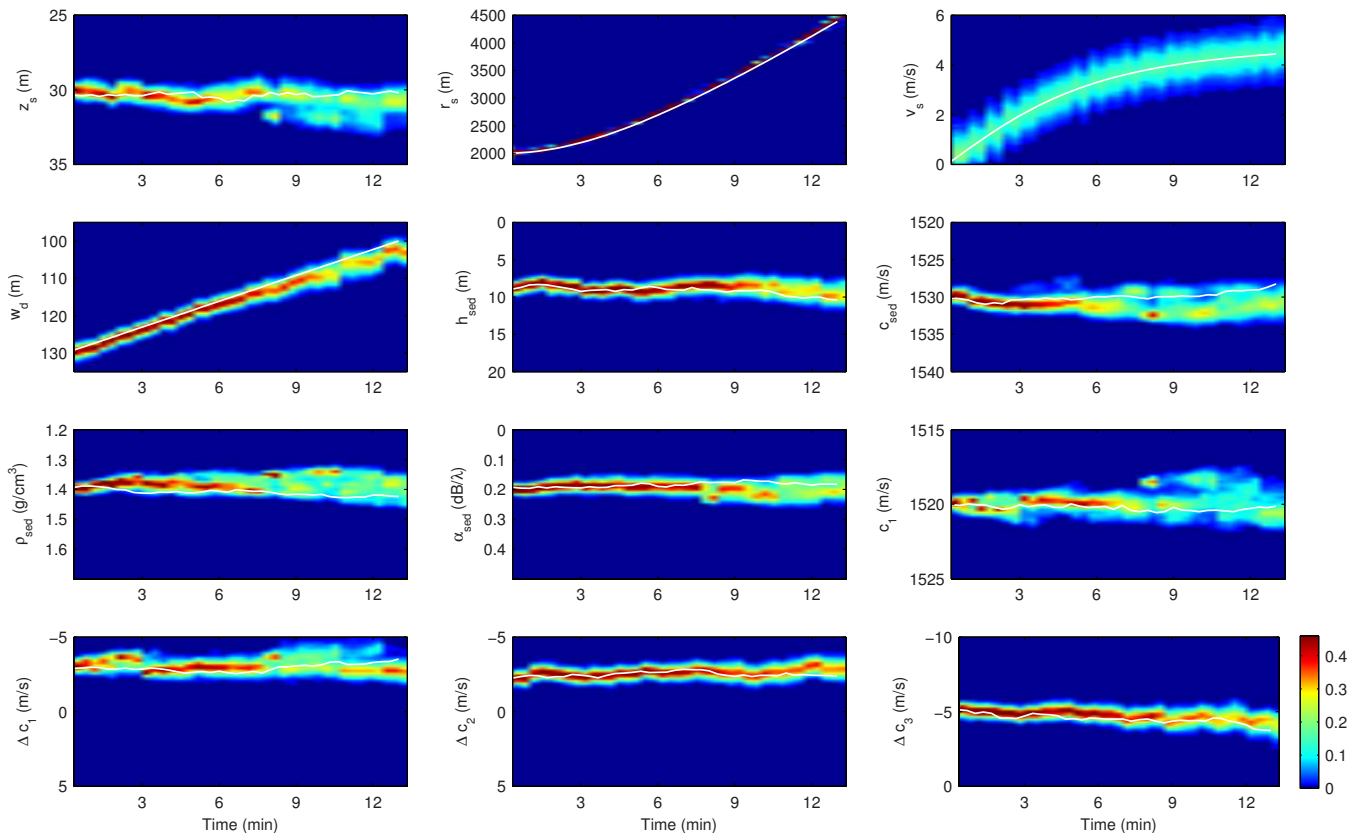| | |
|---|---|
| Receiver type | VLA |
| No. of hydrophones | 24 |
| First/last element depth | 26/118 m |
| PF size | 10 000 |
| Water depth at VLA location | 130 m |
| Water depth at source location | 100–130 m |
| Source frequencies | 200, 275, 350, 425 Hz |
| SNR at $r = 2.0$ km ($\mathbf{R}_0$) | 8.8 dB |
| SNR at $r = 4.4$ km ($\mathbf{R}_{40}$) | 3.1 dB |
| Track length | 13.3 min ($k = 40$) |
| Sampling interval, $\Delta t$ | 20 s |
| Radial source speed | 0–5 m/s |

FIG. 2. (Color online) Time evolving marginal posterior PDF normalized histograms of particles for the geoacoustic PF simulation and the true trajectory (solid white) of each parameter. The values are in terms of probability/bin with each vertical slice adding up to 1.

has little sensitivity to sediment density, top layer sound speed, and bottom parameters. Due to their negligible affect on the measured field, the bottom parameters are not tracked.

The initial environment at $t=0$ has a Gaussian PDF with a variance $\mathbf{P}_0$ given in Table I. Three simulations are performed where the error in the source location is used as a metric of overall track performance as follows.

(1) *Geoacoustic and source tracking PF*. A PF that tracks the geoacoustic and source parameters simultaneously.
(2) *Mismatched MFP*. A standard MFP inversion that does not update the changes in the environment and uses the environment at $t=0$ for successive source localizations. Therefore, no environmental parameter is inverted. No tracking filter is used. This sequential inversion shows how the source parameters are affected when the environmental parameters are not tracked.
(3) *Mismatched (source tracking only) PF*. A PF that tracks only the three source parameters, ignoring the changes in the environment, similar to the mismatched MFP case. Only source parameters are used in the state equation and no geoacoustic tracking is performed. This simulation shows the effects of environmental mismatch on a particle filter tracking algorithm.

The results of the geoacoustic and source tracking PF are given in Figs. 2–4. Since the purpose is to demonstrate how the PF tracks the evolving uncertainties in parameters as PPDs, a large number of particles is used to obtain smooth histograms that represent them. Each particle has the same

weight after resampling, therefore, a histogram of these particles approximates the PPD up to a multiplicative constant. Hence, the uncertainties are given in terms of normalized histograms of particles where each bin is computed using the number of resampled particles in that bin divided by the total number of particles.

The evolution of the 1-D marginal posterior densities are given in Fig. 2. The plots in the first row belong to the source parameters. For all three source parameters, the 1-D marginal PPDs follow the true parameter trajectories. Due to the ability of the geoacoustic PF to correct for the variations in the environment, the source range is tracked with a low rms error. The source depth PPD becomes non-Gaussian at large $t$ where the ship is further from the VLA resulting in a lower SNR. Variation in the radial source velocity is also well-tracked even with the selected constant velocity evolution model. The environmental parameter tracks are in rows 2–4. Many of the PPDs become non-Gaussian and some of the parameters are tracked better than others. A vertical slice from each of the evolving PPDs in Fig. 2 is given in Fig. 3 for $t=10$ min. This snapshot shows how some parameters such as $h_{sed}$, $v_s$, $\Delta c_2$ and $\Delta c_3$ are tracked better than others that are either less sensitive ($\rho_{sed}$, $\alpha_{sed}$, $c_1$) or quickly changing parameters ($w_d$).

Since the SSP is downward refracting, more acoustic energy is in the lower water column, interacting with the sediment. This is in agreement with the sensitivity curves in Fig. 1(c) with $\Delta c_1$ being the least sensitive and $\Delta c_3$ being the most because of the refractive profile. The effects of this on
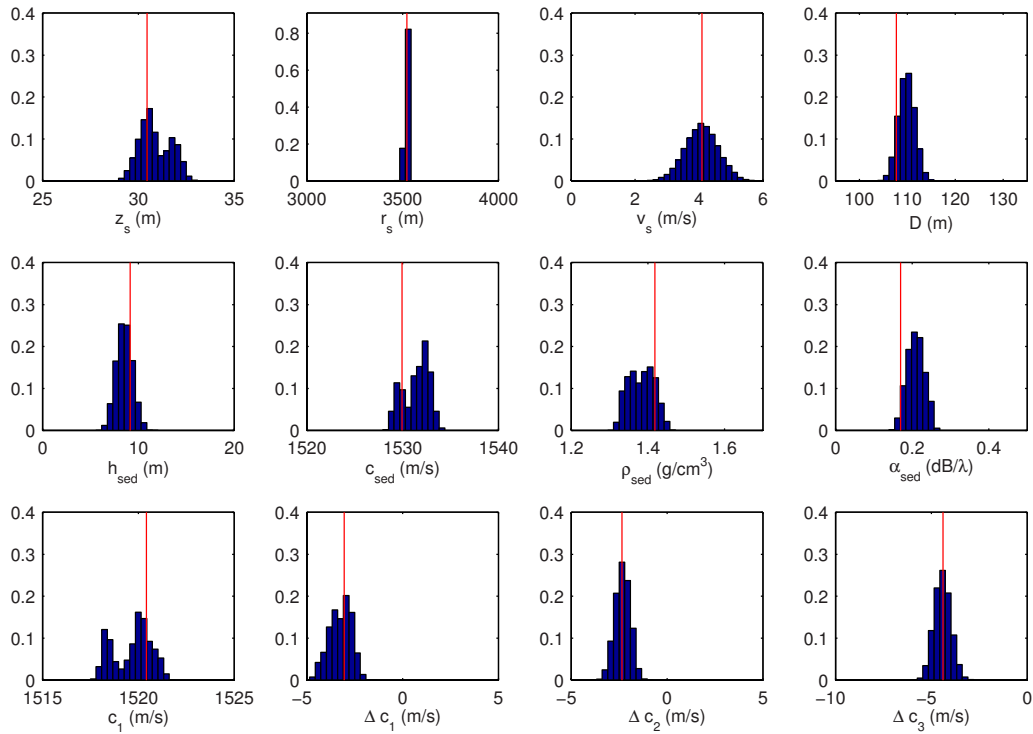
FIG. 3. (Color online) Normalized histograms of the particles approximating the 1-D PPD of all source and environmental parameters at $t=10$ min. Vertical lines show the true values. $Y$-axis is in terms of probability/bin.

the PF performance can be observed directly by comparing the evolving PPDs and their variances. $c_1$ and $\Delta c_1$ are the least well-tracked parameters with highly non-Gaussian PDFs and large variances, whereas $\Delta c_3$ is well-tracked at all



FIG. 4. (Color online) 2-D depth-range normalized histograms of the moving source at time $t=5,10$, and 13.3 min. '○' represents the true source location. Values are in terms of probability/bin.

times with a sharp density. The PPDs of many of the parameters become wider as $t$ increases due to the decreasing SNR.

The only environmental parameter that is changing fast is the water depth $w_d$ at the source location. Figure 2 shows that $w_d$ is tracked well enough for source to be tracked accurately, even though the environmental state equation assumes a slowly changing environment with $E(\mathbf{m}_{k+1}) = E(\mathbf{m}_k)$. As the PF can operate with non-Gaussian, multimodal PDFs, it turns out to be a good choice given the variety of densities obtained in Fig. 3, such as the posterior PDFs for $z_s$, $c_{\text{sed}}$, and $c_1$.

The evolution of the 2-D PPD of the source depth/range at three time steps is given in Fig. 4. The ability to track both the geoacoustic parameters and the source enables the geoacoustic and source tracking PF to track accurately the source with a small variance in range and depth. The results at the mid point and the end of the track are given in Table III. This PF makes only 0.1 m, 1 m, and less than 0.1 m/s error at the
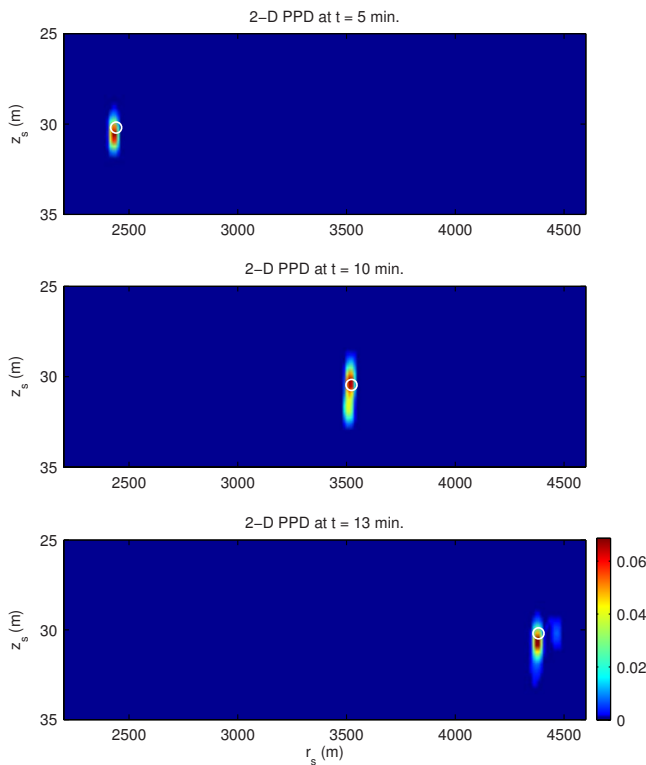
TABLE III. Results.

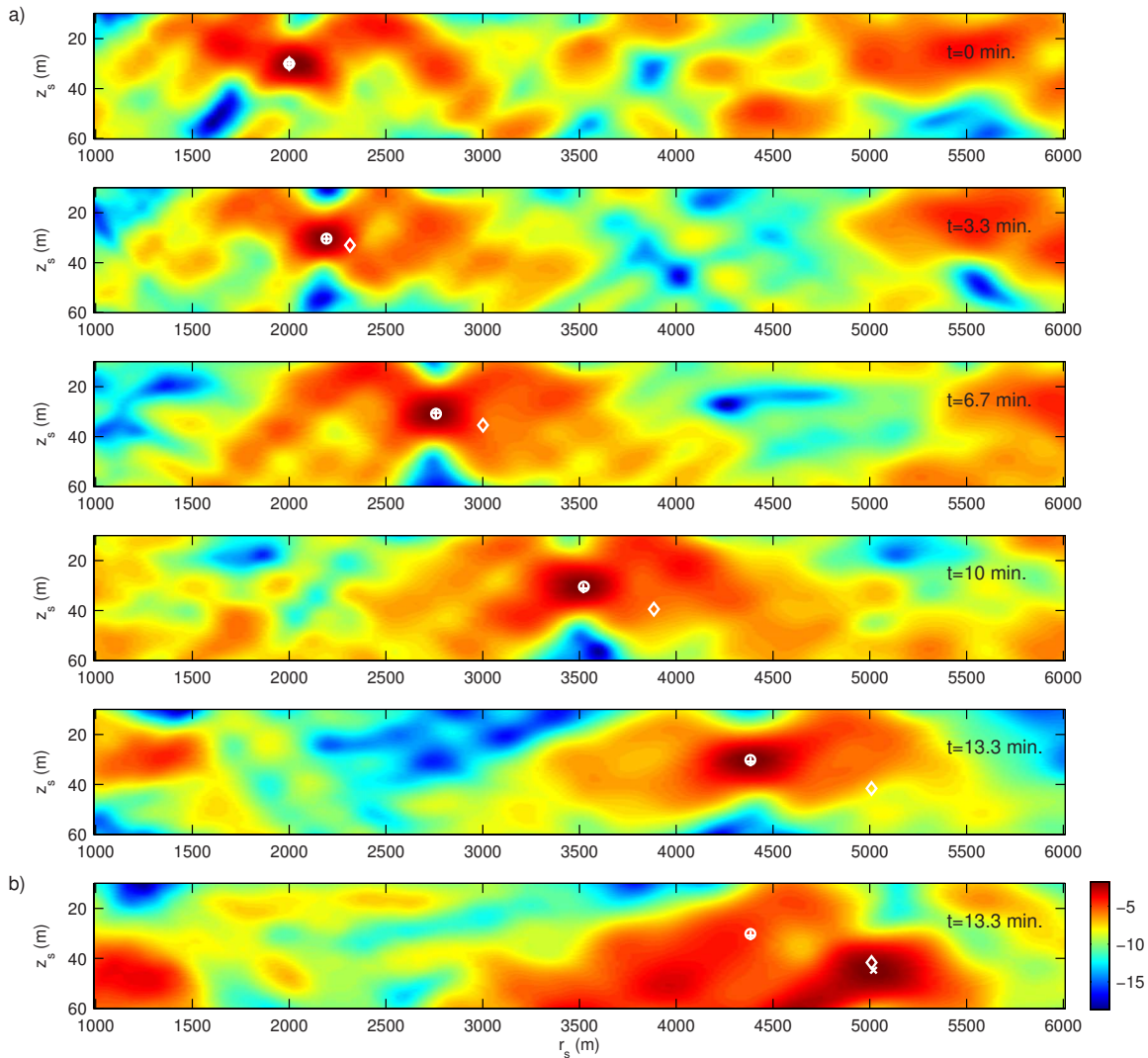| $t$ (min) | Method | $z_s$ (m) | $r_s$ (m) | $v_s$ (m/s) |
|---|---|---|---|---|
| 6.7 | True value | 30.6 | 2691 | 3.3 |
| | Geoacoustic PF | 30.5 | 2690 | 3.3 |
| | Mismatched MFP | 35.7 | 2941 | ⋯ |
| | Mismatched PF | 34.9 | 2934 | 3.1 |
| 13.3 | True value | 30.2 | 4383 | 4.4 |
| | Geoacoustic PF | 30.8 | 4385 | 4.5 |
| | Mismatched MFP | 44.7 | 5020 | ⋯ |
| | Mismatched PF | 41.7 | 5009 | 6.5 |

FIG. 5. (Color online) (a) Geoacoustic and source tracking PF (+) and mismatched (source tracking only) PF (◇) at $t=0,3.3,6.7,10,13.3$ min ($k$ $=0,10,20,30,40$), respectively. Background is the normalized MFP ambiguity surface (dB) for the true environment. 'o' is the true source location. (b) Results at $t=13.3$ min where the background is the mismatched-MFP (dB) that uses a constant environment ($t=0$ value) with the mirage located at (×).

mid-track for the source depth, range, and speed, respectively. Even after the full track length 0f 13.3 min., the error terms stay at 0.6 m, 2 m, and 0.1 m/s.

When there is a mismatch between the assumed water depth and its actual value, the source appears at a different location which is known as the source mirage effect.[30,31] The bathymetry changes from initially flat (at 130 m) to a sloped-bottom as the ship moves into shallower water finally reaching a water depth of 100 m. Ignoring this variation results in a mirage forming after $t=0$ and slowly moving away from the true location. Figure 5 shows such a mismatched MFP estimator using a normalized Bartlett mismatch [Eq. (11)].

In an ideal waveguide with pressure release boundaries, the ratio of MFP range estimate to true source range is equal to the ratio of flat bathymetry water depth to true water depth at source location, creating a mirage.[31] The same ratio is valid for source depth regardless of the frequency used. Since the actual environment used here is more complex with a sedimentary layer these relations are approximate. Nevertheless, a mirage is formed 637 m further away and 14.5 m deeper than the true source at $t=13.3$ min [× in Fig. 5(b)].

To show that the inclusion of the environmental parameters improves tracking of the source location, a mismatched (source tracking only) PF is used with the environment at $t$ $=0$ (◇ in Fig. 5). This PF tracks the slowly diverging mirage with a posterior value close to the mismatched-MFP maxima at all times, see Fig. 5(b). In contrast, the geoacoustic and source tracking PF tracks the true source range and depth for all $t$. This is observed clearly from the evolution of the three source parameters given in Fig. 6.

It is interesting to note that, by running the mismatched PF and the geoacoustic and source tracking PF together it is possible to track both the source and the mirage and the error between them. This provides an estimate for the rate at which one must perform a geoacoustic inversion to update the current values of the environmental parameters in order to successfully track the source using source only tracking algorithms.

### B. SWellEx-96 experiment

The particle filter is used on acoustic data collected during the shallow water evaluation cell experiment

82    J. Acoust. Soc. Am., Vol. 128, No. 1, July 2010

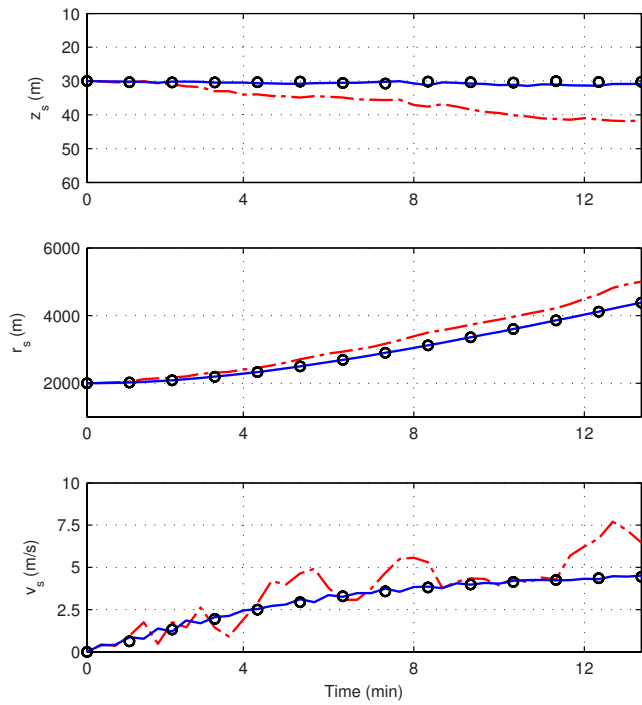Yardim et al.: Geoacoustic and source tracking

FIG. 6. (Color online) Track results of three source parameters for geoacoustic and source tracking PF (solid) vs mismatched (source tracking only) PF (dashed), together with the true trajectory ($\bigcirc$).
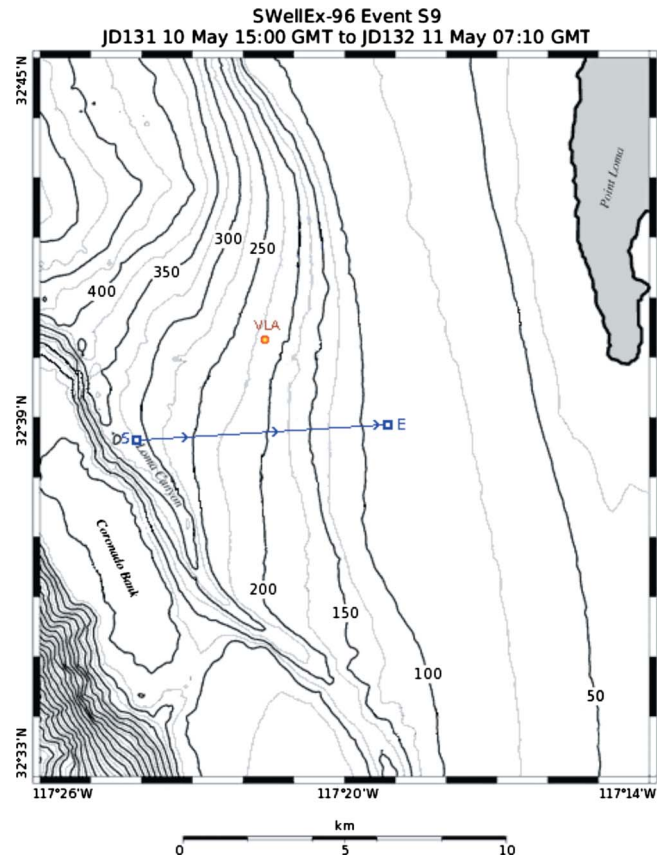


FIG. 7. (Color online) Bathymetry (in meters) of the SWellEx-96 area, VLA (R/P FLIP), and the west-east source track for event S9.

(SWellEx-96).[32] It was conducted in May 1996, off the coast of San Diego, CA, near Point Loma. A VLA with specifications given in Table IV was deployed from R/P Flip at 216.5 m deep water north of Loma Canyon. Event S9 is selected here since the track is perpendicular to bathymetric lines giving the highest rate of change of environment as ship moves into shallower waters (Fig. 7).[33] The source is towed at 2.6 m/s at a depth of 55 m. The source is a comb signal composed of 13 frequencies from 49–388 Hz (see Table IV). The water column sound speed profile is provided by conductivity-temperature-depth (CTD) measurements.

The environmental variation at the moving source location is seen in Fig. 8(a).[33] Three range-dependent environments along the track are given in Figs. 8(b) and 8(d).[33] These propagation paths are only moderately complex and are approximated by linearly interpolating the modes at the locations of the source and the VLA. Therefore, the adiabatic normal mode model SNAPRD (Ref. 23) is used. This assumes all energy in a given mode at source location transfers to the

corresponding mode at the VLA environment, neglecting cross coupling terms.[34] An environmental model given in Fig. 9 is adopted at the location of source and VLA. The environment at the fixed VLA location is assumed known and the environment at the moving source location is tracked.
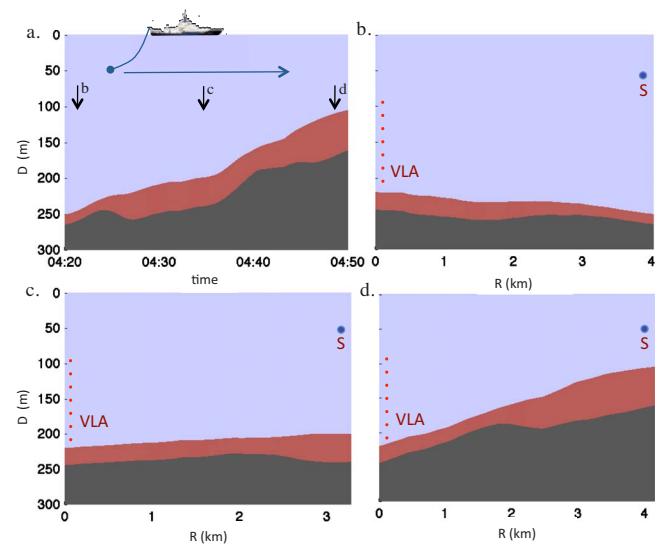


FIG. 8. (Color online) (a) The 30 min section of the bathymetry and the sediment properties along the source track. The range-dependent acoustic propagation path between the moving source and the VLA at (b) start of the track, (c) mid-track, and (d) end of the track.

TABLE IV. SWellEx-96: experimental setup.

| FLIP/VLA | |
| --- | --- |
| Position | 32°40.254′ N, 117°21.620′ W |
| First/last element | 212.25/94.125 m |
| Aperture | 118 m |
| No. of elements used | 21 |
| Sampling rate | 1500 Hz |
| SPROUL/towed source | |
| Frequencies | 49, 64, 79, 94, 112, 130, 148, 166, 201, 235, 283, 338, 388 Hz |

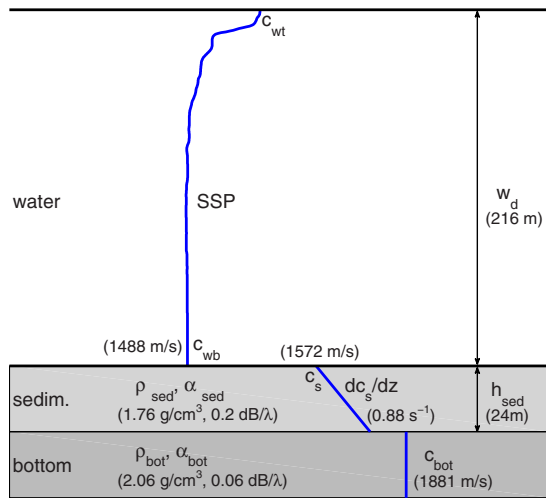Yardim *et al.*: Geoacoustic and source tracking    83

FIG. 9. (Color online) The environmental parameters used to model the vertical profiles at VLA and source for event S9. The values in parentheses are at the location of the VLA.

To do MFP, cross-spectral density matrices (CSDMs) are estimated for each frequency at each inversion/track step (13 CSDMs in total for each 1 min section). The CSDMs are computed with snapshots of 8192 point FFTs with 50% overlap between successive FFTs. This enabled us to compute the Bartlett power, hence, the likelihood [Eq. (10)] at each step and for each particle in the PF.

The results are given in Fig. 10. It shows two different sequential geoacoustic inversions (no tracking filters) and the results from the geoacoustic and source tracking particle filter along with the known environmental and source parameters. The data analyses and ground truth values were obtained as follows.

(1) The source range values were calculated using the ship GPS. The source starts about 4.5 km away and the range drops to a little over 3 km in the mid track increasing back to 4 km. The VLA tilt relative to the source direction slowly increases from $-1°$ to $-6°$. Water depth was taken from the bathymetry[33] database. The source moves toward the land and the water depth changes from about 250 to 100 m over the 30 min. source track. The sediment parameters were obtained from the mean grain size and the two-way travel time, see Appendix.

(2) The best and worst case scenarios are given by the two sequential inversions. The acoustic data were inverted using two sequential genetic algorithm (GA) runs. Each GA run inverts the data at each step (1 min) using 15 000 forward model runs per $k$. One represents the best case scenario by assuming the environments both at the source and VLA locations are known (values taken from Appendix) at every step and the only unknown are source depth, range, and VLA tilt. This sets the upper limit for the geoacoustic and source tracking PF performance. The other one represents a sequential inversion that has no geoacoustic information other than the known environment at the VLA location and hence uses a range-independent model with values given in Fig. 9. This shows how much error in source localization one can make by ignoring the effects of the range-dependent environment.

(3) The source was tracked along with the environmental parameters using a 200-particle PF. The state vector was composed of eight parameters, four representing source and VLA parameters (source depth, range, radial speed, and VLA tilt) and four representing the environment at the source location (water depth, $h_{sed}$, $c_s$, and $dc_s/dz$).
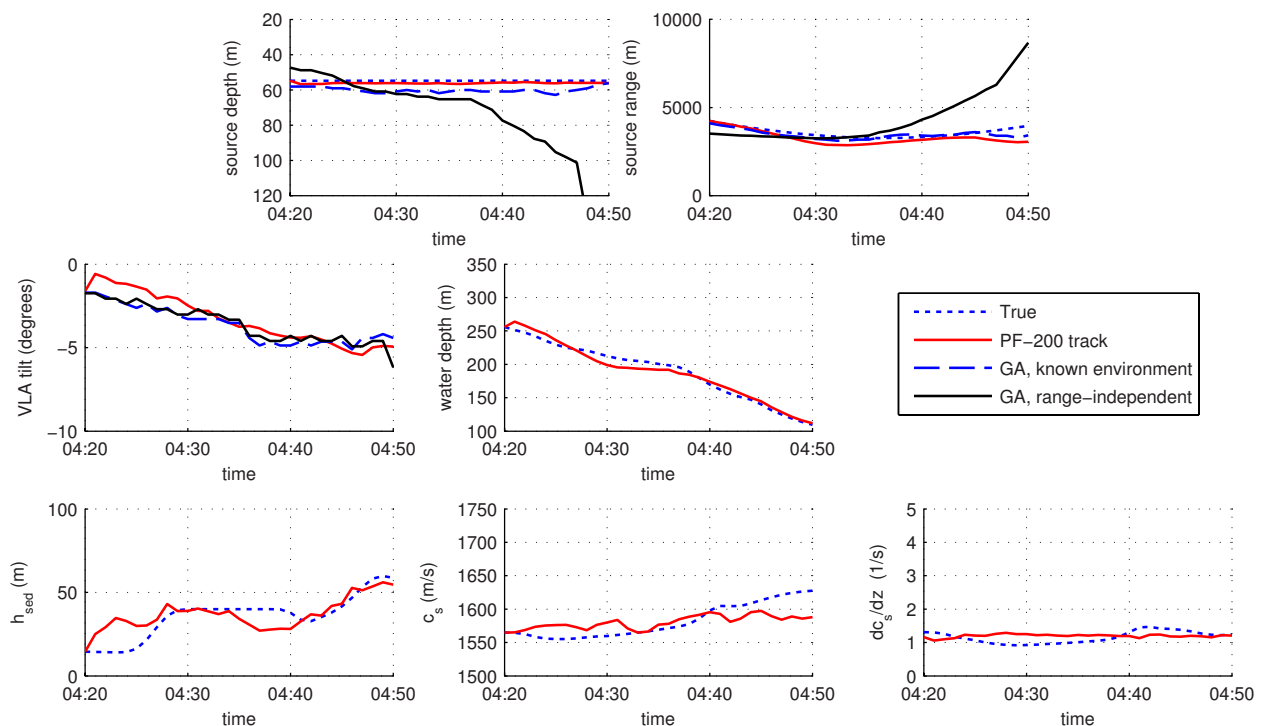


FIG. 10. (Color online) Track results for the geoacoustic and source parameters for event S9, together with the true trajectories.

TABLE V. SWellEx-96: PF initiation.

| x | $\mathbf{P}_0^{1/2}$ | State noise, $\mathbf{Q}_k^{1/2}$ |
|---|---|---|
| $z_s$ (m) | 2 | 0.25 |
| $r_s$ (m) | 50 | $0.01 \times \dfrac{\Delta t^2}{2}$ |
| $v_s$ (m/s) | 0.5 | $0.01 \times \Delta t$ |
| VLA tilt (°) | 0.4 | 0.3 |
| $w_d$ (m) | 10 | 5 |
| $h_{sed}$ (m) | 10 | 5 |
| $c_s$ (m/s) | 20 | 5 |
| $dc_s/dz$ (1/s) | 0.2 | 0.05 |

Similar to the example in Sec. IV A, these environmental parameters were selected based on a sensitivity analysis showing that the Bartlett power is not sensitive to attenuation and density in the sediment at the source location, and basement parameters. The method used here assumes we know the environment at the fixed array location and we are only tracking the environment below the moving source. Hence some of the parameters such as the density and attenuation at the array location are already known. Therefore, the objective function is less sensitive to the value at the source location compared to performing an inversion for a fully unknown range-independent attenuation or density value. The track was initiated using the results of a full environmental and source parameter GA inversion performed at the first time index. The prior standard deviations and the state noise were selected as given in Table V. Selection of suitable noise covariances for the PF is essential to tune the filter. In acoustic applications, the $\mathbf{R}_k$ is directly related to the noise in the measurement and can be inferred from the SNR but the state noise $\mathbf{Q}_k$ is not a directly observable noise term.

Changing this value can result in different filter performance. Selection of $\mathbf{Q}_k$ is a trade-off between how much we trust the evolution model given in the state equation and how noisy an estimate we want. Large $\mathbf{Q}_k$ can capture sudden changes in the state parameters (Ref. 1 shows this by tracking the sea bottom parameters through a sudden sediment thickness and sound speed jump) but by their nature a large noise term will make the estimates noisy. The values used in Table V are chosen to try to strike the balance between these two. The initial densities for parameters are selected as relatively broad Gaussian priors with $\mathbf{P}_0$ consistent with what one would get from a typical geoacoustic inversion.

The mismatch between the best case inversion that uses true range-dependent environment and the range-independent assumption of the worst case inversion exhibits itself as a mirage similar to the simulation in Sec. IV A. The larger the environmental mismatch gets, the greater the error in the source depth and range becomes. At the beginning of the track the water depth at the source is more than the 216 m used in the range-independent profile, creating a side lobe at a shallower and closer point.[31] Likewise, toward the end of
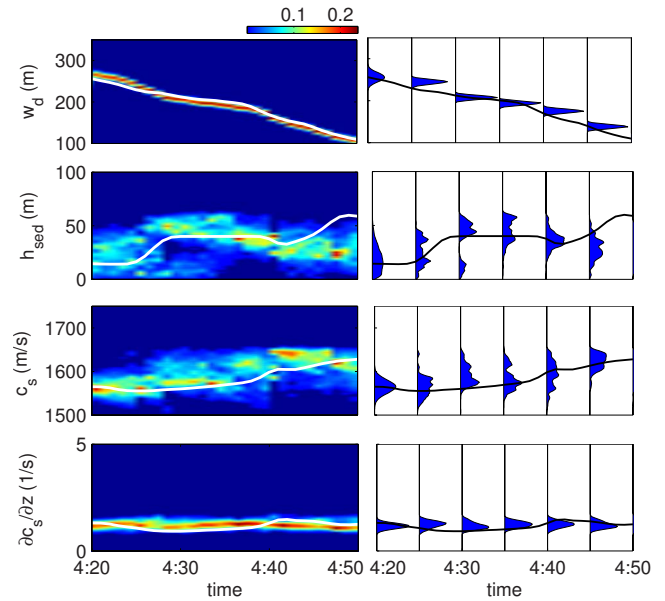


FIG. 11. (Color online) Evolving marginal posterior PDFs for the geoacoustic parameters. Vertical slices of the PDFs are given at every 5 min intervals. Solid lines represent the true values.

the track the water depth at the source is shallower and hence the worst case inversion predicts a source deeper and farther away than the true location.

Most of this error is mitigated by including the true environment at the source location as shown in the best case results with the known environment. Therefore, if a geoacoustic and source tracking PF or sequential optimization algorithm inverts the environment accurately, the errors introduced into source localization by the mismatched environment in the MFP will be minimized. Then, this algorithm should ideally be able to match the source localization quality of the best-case scenario when the actual environment is known.

The results of the geoacoustic and source tracking PF in Fig. 10 closely follows the results of the best case inversion with source depth-range estimates close to the GPS measurements. The PF is able to track the source only using 200 particles (200 forward model runs per step), significantly less than the GAs that run 15 000 forward models per step. This is because the PF uses not only the current data but also the previous parameter estimates which reduce significantly the search space for the parameters at the next step.

Uncertainty analysis is performed next. Even though the source is successfully tracked by using a 200-particle PF, a second filtering is performed using a 10 000-particle PF. This enables us to obtain much better histograms of particles that represent the marginal posterior PDFs of the geoacoustic parameters. Evolving marginal posterior PDFs of the four geoacoustic parameters are given in Fig. 11. The water depth is well determined throughout the track and the posterior PDFs correspond to narrow Gaussian PDFs. The slope of the sediment sound speed profile is likewise well-determined, closely following the underlying true values obtained using the Bachman database. Note, however, that both the sedi-
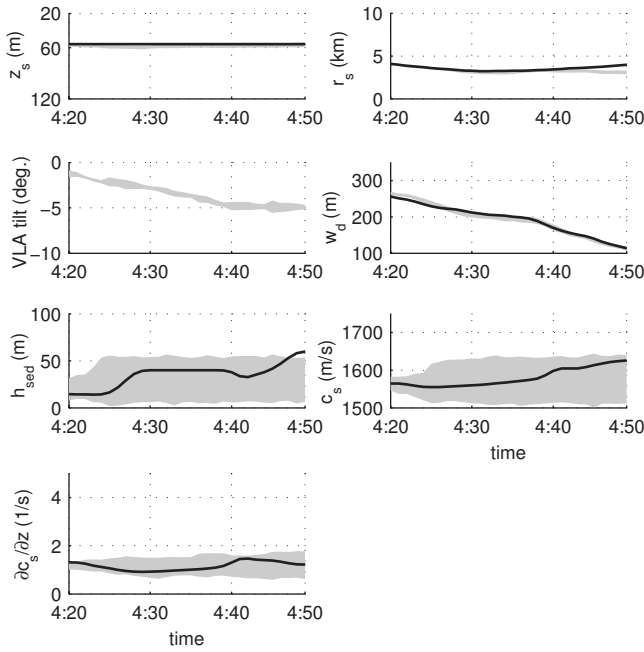
FIG. 12. Range of values observed during filtering for geoacoustic and source parameters based on 100 PF-200 runs. Solid lines represent the true values.

ment thickness and top layer sound speed have highly non-Gaussian, quickly evolving posterior PDFs with multiple peaks.

The range of values obtained for both source and geoacoustic parameters are given in Fig. 12 based on 100 PF-200 runs. Note that both the source range and depth, VLA tilt, and water depth fluctuate in very tight ranges, closely following the true underlying values. In contrast, $h_{sed}$ changes between 10–55 m, $c_s$ from 1500–1640 m/s, and the slope of the sediment sound speed between 0.8–1.8 $s^{-1}$. The relatively large uncertainties observed both in Figs. 11 and 12 for sediment properties might be related to the bathymetry and sediment profiles given in Fig. 8. Since only environments at source and receiver are used, complicated changes cannot be modeled. The profiles given in Figs. 8(b)–8(d) do not always conform to that simple model, resulting in modeling errors that get projected into the inversion as uncertainty in the parameters. For example, in Fig. 8(d), the sediment thickness in almost constant from 0–2 km and then quickly doubles and stays flat from 2.5–4 km.

## V. SUMMARY

This paper has addressed the tracking of geoacoustic parameters during an environmental survey (e.g., water column SSP, water depth, sediment and bottom parameters), together with acoustic source parameters (e.g., source depth, range and speed) in spatially and/or temporally changing ocean acoustic environments. For this purpose, a PF approach has been adopted where the environmental parameters are tracked simultaneously with the source location and ship speed in a range-dependent environment. The need to analyze the sequential stream of acoustic data in real-time, the nonlinearity between the source/environmental parameters and the measured acoustic field, and the non-Gaussian

PPDs typically encountered in geo-acoustic inversions makes particle filters an attractive complement to other techniques used in geoacoustic inversion and source localization.

The PF tracks the environmental and source parameters together with their underlying uncertainties in the form of a time evolving PPD. The capabilities of the approach were demonstrated in simulation for an environment with evolving water depth, sound speeds, density and attenuation values, and sediment thicknesses. The PF tracked correctly the environment together with the source location.

Then the PF was applied successfully to data collected during the SWellEx-96 experiment. The PF tracked both the environmental parameters and the source in a range-dependent shallow water environment with performance close to that of carrying out source tracking alone where the environment is known.

## APPENDIX: EXTRACTION OF SEDIMENT PARAMETERS FROM BACHMAN DATABASE

Bachman et al.[33] produced a seabed geologic model that is a gridded database containing water depth, sediment grain size, sediment thickness, and acoustic basement type. Grid cells are squares of side length equal to 2 arc seconds ($\sim$60 m). The sediment thickness and sound speed profile are obtained from the mean grain size database[33] provided in terms of $\overline{gs} = -\log_2$ (mean grain size in mm). This is done by first computing the sound speed ratio (SSR) between the water sound speed and the sediment sound speed at the sediment-water interface[35]

$$SSR = 1.18 - 0.034\overline{gs} + 0.0013\overline{gs}^2, \tag{A1}$$

$$c_{sed}(0) = SSR \times c_{wb}. \tag{A2}$$

$c_{wb}$ is the bottom water sound speed and $c_{sed}(0)$ is the sediment sound speed at sea floor. Then two sediment sound speed profiles are constructed as a function of depth for a sandy[36] sediment ($\overline{gs} \leq 3.25$) and a sediment with silts and clays[37] ($\overline{gs} \geq 5.75$). The sediment with a $\overline{gs}$ between these two values is approximated to behave as a weighted average. Therefore, the sediment sound speed profile as a function of depth is given by

$$c_{sand}(z) = c_{sed}(0) \times \left(\frac{z}{0.05}\right)^{0.015}, \tag{A3}$$

$$c_{silt}(z) = c_{sed}(0) + 0.712z, \tag{A4}$$

$$w_{silt} = \frac{\overline{gs} - 3.25}{5.75 - 3.5}, \quad w_{sand} = 1 - w_{silt}, \tag{A5}$$

$$c_{sed}(z) = w_{sand}c_{sand}(z) + w_{silt}c_{silt}(z), \tag{A6}$$

where $z$ is depth relative to the sea floor. Sediment thickness $h_{sed}$ is obtained from two-way travel time (i.e., sea floor to

Yardim et al.: Geoacoustic and source tracking

basement and back to sea floor) by integrating the sound speed profile given above.

This sediment sound speed profile is simplified by linearizing it for the tracking and inversion algorithms used in this paper. Hence, it is represented by only two parameters, $c_s$ and the slope $dc_s/dz$. $c_s$ is defined as the mean of sediment sound speed profile within the top 5 m and the slope is calculated by $(c_{sed}(h_{sed}) - c_s)/h_{sed}$. Along the path of the source, both sediment thickness $h_{sed}$ and top layer sound speed $c_s$ gradually increase from 10 to 50 m and from 1570 to 1620 m/s, respectively. The slope $dc_s/dz$ fluctuates around 1 s$^{-1}$.

[1]C. Yardim, P. Gerstoft, and W. S. Hodgkiss, "Tracking of geoacoustic parameters using Kalman and particle filters," J. Acoust. Soc. Am. **125**, 746–760 (2009).

[2]L. Sha and L. W. Nolte, "Effects of environmental uncertainties on sonar detection performance prediction," J. Acoust. Soc. Am. **117**, 1942–1953 (2005).

[3]C.-F. Huang, P. Gerstoft, and W. S. Hodgkiss, "Validation of statistical estimation of transmission loss in the presence of geoacoustic inversion uncertainty," J. Acoust. Soc. Am. **120**, 1932–1941 (2006).

[4]R. L. Culver and H. J. Camin, "Sonar signal processing using probabilistic signal and ocean environmental models," J. Acoust. Soc. Am. **124**, 3619–3631 (2008).

[5]L. Sha and L. W. Nolte, "Bayesian sonar detection performance prediction with source position uncertainty using SWellEx-96 vertical array data," IEEE J. Ocean. Eng. **31**, 345–355 (2006).

[6]P. Gerstoft, "Inversion of seismoacoustic data using genetic algorithms and *a posteriori* probability distributions," J. Acoust. Soc. Am. **95**, 770–782 (1994).

[7]S. E. Dosso, "Quantifying uncertainty in geoacoustic inversion I. A fast Gibbs sampler approach," J. Acoust. Soc. Am. **111**, 129–142 (2002).

[8]N. R. Chapman, S. Chin-Bing, D. King, and R. B. Evans, "Benchmarking geoacoustic inversion methods for range-dependent waveguides," IEEE J. Ocean. Eng. **28**, 320–330 (2003).

[9]D. P. Knobles, R. A. Koch, L. A. Thompson, K. C. Focke, and P. E. Eisman, "Broadband sound propagation in shallow water and geoacoustic inversion," J. Acoust. Soc. Am. **113**, 205–222 (2003).

[10]A. M. Richardson and L. W. Nolte, "A posteriori probability source localization in an uncertain sound speed, deep ocean environment," J. Acoust. Soc. Am. **89**, 2280–2284 (1991).

[11]M. D. Collins and W. A. Kuperman, "Focalization: Environmental focusing and source localization," J. Acoust. Soc. Am. **90**, 1410–1422 (1991).

[12]S. E. Dosso and M. J. Wilmut, "Comparison of focalization and marginalization for Bayesian tracking in an uncertain ocean environment," J. Acoust. Soc. Am. **125**, 717–722 (2009).

[13]S. E. Dosso and M. J. Wilmut, "Uncertainty estimation in simultaneous Bayesian tracking and environmental inversion," J. Acoust. Soc. Am. **124**, 82–97 (2008).

[14]J. V. Candy and E. J. Sullivan, "Passive localization in ocean acoustics: A model-based approach," J. Acoust. Soc. Am. **98**, 1455–1471 (1995).

[15]E. J. Sullivan, J. D. Holmes, W. M. Carey, and J. F. Lynch, "Broadband passive synthetic aperture: Experimental results," J. Acoust. Soc. Am. **120**, EL49–EL54 (2006).

[16]J. V. Candy, *Bayesian Signal Processing: Classical, Modern and Particle Filtering Methods* (Wiley, Hoboken, NJ, 2009).

[17]O. Carrière, J.-P. Hermand, J.-C. Le Gac, and M. Rixen, "Full-field tomography and Kalman tracking of the range-dependent sound speed field in a coastal water environment," J. Mar. Syst. **78**, S382–S392 (2009).

[18]C. He, J. E. J. E. Quijano, and L. M. Zurk, "Enhanced Kalman filter algorithm using the invariance principle," IEEE J. Ocean. Eng. **34**, 575–585 (2009).

[19]O. Carrière, J. Hermand, M. Meyer, and J. V. Candy, Dynamic Estimation of the Sound-Speed Profile From Broadband Acoustic Measurements (Oceans, 2007).

[20]O. Carrière, J.-P. Hermand, and J. V. Candy, "Inversion for time-evolving sound-speed field in a shallow ocean by ensemble Kalman filtering," IEEE J. Ocean. Eng. **34**, 586–602 (2009).

[21]I. Zorych and Z.-H. Michalopoulou, "Particle filtering for dispersion curve tracking in ocean acoustics," J. Acoust. Soc. Am. **124**, EL45–EL50 (2008).

[22]B. Ristic, S. Arulampalam, and N. Gordon, *Beyond the Kalman Filter: Particle Filters for Tracking Applications* (Artech House, Boston, MA, 2004).

[23]P. Gerstoft, "SAGA Users guide 5.0, an inversion software package, an updated version of 'SAGA 2.0'," Report No. SM-333, SACLANT Undersea Research Centre, La Spezia, Italy, 1997.

[24]F. B. Jensen and M. C. Ferla, "SNAP: The SACLANTCEN normal-mode acoustic propagation model," Report No. SM-121, SACLANT Undersea Research Centre, La Spezia, Italy, 1979.

[25]N. J. Gordon, D. J. Salmond, and A. F. M. Smith, "Novel approach to nonlinear/non-Gaussian Bayesian state estimation," IEE Proc. F, Radar Signal Process. **140**, 107–113 (1993).

[26]J. J. K. Ó. Ruanaidh and W. J. Fitzgerald, *Numerical Bayesian Methods Applied to Signal Processing, Statistics and Computing Series* (Springer-Verlag, New York, 1996).

[27]C. F. Mecklenbräuker and P. Gerstoft, "Objective functions for ocean acoustic inversion derived by likelihood methods," J. Comput. Acoust. **8**, 259–270 (2000).

[28]Z.-H. Michalopoulou, "The effect of source amplitude and phase in matched field source localization," J. Acoust. Soc. Am. **119**, EL21–EL26 (2006).

[29]C.-F. Huang, P. Gerstoft, and W. S. Hodgkiss, "Uncertainty analysis in matched-field geoacoustic inversions," J. Acoust. Soc. Am. **119**, 197–207 (2006).

[30]D. R. Del Balzo, C. Feuillade, and M. M. Rowe, "Effects of water-depth mismatch on matched-field localization in shallow-water," J. Acoust. Soc. Am. **83**, 2180–2185 (1988).

[31]G. L. D'Spain, J. J. Murray, W. S. Hodgkiss, N. O. Booth, and P. W. Schey, "Mirages in shallow water matched field processing," J. Acoust. Soc. Am. **105**, 3245–3265 (1999).

[32]N. O. Booth, A. T. Abawi, P. W. Schey, and W. S. Hodgkiss, "Detectability of low-level broad-band signals using adaptive matched-field processing with vertical aperture arrays," IEEE J. Ocean. Eng. **25**, 296–313 (2000).

[33]R. T. Bachman, P. W. Schey, N. O. Booth, and F. J. Ryan, "Geoacoustic databases for matched-field processing: Preliminary results in shallow water off San Diego, California," J. Acoust. Soc. Am. **99**, 2077–2085 (1996).

[34]F. B. Jensen, W. A. Kuperman, M. B. Porter, and H. Schmidt, *Computational Ocean Acoustics* (American Institute of Physics, New York, 1994).

[35]M. D. Richardson and K. B. Briggs, "On the use of acoustic impedance values to determine sediment properties," Proc. Inst. Acous. **15**, 15–23 (1993).

[36]E. L. Hamilton, "Shear-wave velocity versus depth in marine sediments: A review," Geophysics **41**, 985–996 (1976).

[37]E. L. Hamilton, "Sound-velocity as a function of depth in marine sediments," J. Acoust. Soc. Am. **78**, 1348–1355 (1985).